PixMix: Dreamlike Pictures Comprehensively Improve Safety Measures

Dan Hendrycks[*]
UC Berkeley

Andy Zou[*]
UC Berkeley

Mantas Mazeika
UIUC

Leonard Tang
Harvard University

Dawn Song
UC Berkeley

Jacob Steinhardt
UC Berkeley

Abstract

In real-world applications of machine learning, reliable and safe systems must consider measures of performance beyond standard test set accuracy. These other goals include out-of-distribution (OOD) robustness, prediction consistency, resilience to adversaries, calibrated uncertainty estimates, and the ability to detect anomalous inputs. However, improving performance towards these goals is often a balancing act that today's methods cannot achieve without sacrificing performance on other safety axes. For instance, adversarial training improves adversarial robustness but sharply degrades other classifier performance metrics. Similarly, strong data augmentation and regularization techniques often improve OOD robustness but harm anomaly detection, raising the question of whether a Pareto improvement on all existing safety measures is possible. To meet this challenge, we design a new data augmentation strategy utilizing the natural structural complexity of pictures such as fractals, which outperforms numerous baselines, is near Pareto-optimal, and comprehensively improves safety measures.

1 Introduction

A central challenge in machine learning is building models that are reliable and safe in the real world. In addition to performing well on the training distribution, deployed models should be robust to distribution shifts, consistent in their predictions, resilient to adversaries, calibrated in their uncertainty estimates, and capable of identifying anomalous inputs. Numerous prior works have tackled each of these problems separately (Madry et al., 2018; Hendrycks and Dietterich, 2019; Guo et al., 2017; Emmott et al., 2015), but they can also be grouped together as various aspects of safety engineering for machine learning (Hendrycks et al., 2021b). Consequently, the properties listed above can be thought of as safety measures.

Ideally, models deployed in real-world settings would perform well on multiple safety measures. Unfortunately, prior work has shown that optimizing for some desirable properties often comes at the cost of others. For example, adversarial training only improves adversarial robustness and degrades classification performance (Tsipras et al., 2018). Similarly, inducing consistent predictions on out-of-distribution (OOD) inputs seems to be at odds with better detecting these inputs, an intuition supported by recent work (Chun et al., 2019) which finds that existing help with some safety metrics but harm others. This raises the question of whether improving all safety measures is possible with a single model.
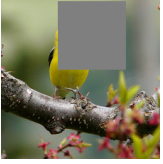
---

[*]Equal Contribution.

Method	Baseline	Cutout	Mixup	CutMix	PIXMIX
Corruptions mCE (↓)	50.0 +0.0	51.5 +1.5	48.0 −2.0	51.5 +1.5	**30.5** −**19.5**
Adversaries Error (↓)	96.5 +0.0	98.5 +1.0	97.4 +0.9	97.0 +0.5	**92.9** −**3.9**
Consistency mFR (↓)	10.7 +0.0	11.9 +1.2	9.5 −1.2	12.0 +1.3	**5.7** −**5.0**
Calibration RMS Error (↓)	31.2 +0.0	31.1 −0.1	13.0 −18.1	29.3 −1.8	**8.1** −**23.0**
Anomaly Detection AUROC (↑)	77.7 +0.0	74.3 −3.4	71.7 −6.0	74.4 −3.3	**89.3** +**11.6**

Table 1: PIXMIX comprehensively improves safety measures, providing significant improvements over state-of-the-art baselines. By contrast, PIXMIX incorporates fractals and feature visualizations into the training process, actively exposing models to new sources of structural complexity.

While previous augmentation methods create images that are different (e.g., translations) or more entropic (e.g., additive Gaussian noise), we argue that an important underexplored axis is creating images that are more complex. As opposed to entropy or descriptive difficulty, which is maximized by pure noise distributions, structural complexity is often described in terms of the degree of organization (Lloyd, 2001). A classic example of structurally complex objects is fractals, which have recently proven useful for pretraining image classifiers (Kataoka et al., 2020; Nakashima et al., 2021). Thus, an interesting question is whether sources of structural complexity can be leveraged to improve safety through data augmentation techniques.

We show that Pareto improvements are possible with PIXMIX, a simple and effective data processing method that leverages pictures with complex structures and substantially improves all existing safety measures. PIXMIX consists of a new data processing pipeline that incorporates structurally complex "dreamlike" images. These dreamlike images include fractals and feature visualizations. We find that feature visualizations are a suitable source of complexity, thereby demonstrating that they have uses beyond interpretability. In extensive experiments, we find that PIXMIX provides substantial gains on a broad range of existing safety measures, outperforming numerous previous methods.

2 Approach

We propose PIXMIX, a simple and effective data augmentation technique that improves many ML Safety (Hendrycks et al., 2021b) measures simultaneously, in addition to accuracy. PIXMIX is comprised of two main components: a set of structurally complex pictures ("Pix") and a pipeline for augmenting clean training pictures ("Mix"). At a high level, PIXMIX integrates diverse patterns from fractals and feature visualizations into the training set. As fractals and feature visualizations do not belong to any particular class, we train networks to classify augmented images as the original class, as in standard data augmentation.

2.1 Picture Sources (PIX)

While PIXMIX can utilize arbitrary datasets of pictures, we discover that fractals and feature visualizations are especially useful pictures with complex structures. Collectively we refer to these two picture sources as "dreamlike pictures." We analyze PIXMIX using other picture sources in the Appendix.
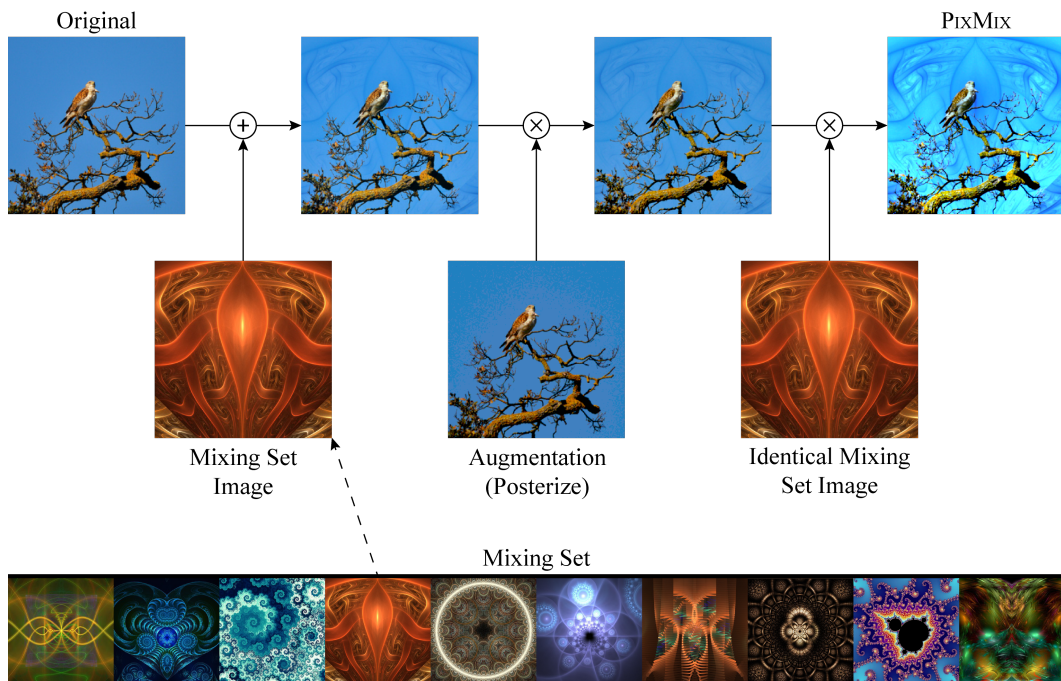
Figure 1: Top: An instance of a PIXMIX augmentation being applied to a bird image. The original clean image is mixed with augmented versions of itself and an image such as a fractal. Bottom: Sample images from the PIXMIX mixing set. We select fractals and feature visualizations from manually curated online sources. In ablations, we find that these new sources of visual structure for augmentations outperform numerous synthetic image distributions explored in prior work (Baradad et al., 2021).

Fractals. Fractals can be generated in several ways, with one of the most common being iterated function systems. Rather than generate our own diverse fractals, which is a substantial research endeavor (Kataoka et al., 2020), we download 14,230 fractals from manually curated collections on DeviantArt. The resulting fractals are visually diverse, which can be seen in the bottom portion of Figure 1.

Feature Visualization. Feature visualizations that maximize the response of neurons create archetypal images for neurons and often have high complexity (Mordvintsev et al., 2015; Olah et al., 2017). Thus, we include feature visualizations in our mixing set. We collect 4,700 feature visualizations from the initial layers of several convolutional architectures using OpenAI Microscope. While feature visualizations have been primarily used for understanding network representations, we connect this line of interpretability work to improve performance on safety measures.

2.2 Mixing Pipeline (MIX)

The pipeline for augmenting clean training images is described in Figure 2. An instance of our mixing pipeline is shown in the top half of Figure 1. First, a clean image has a 50% chance of having a randomly selected standard augmentation applied. Next, we augment the image a random number of times with a maximum of k times. Each augmentation is carried out by either additively or multiplicatively mixing the current image with a freshly augmented clean image or an image from the mixing set. Multiplicative mixing is performed similarly to the geometric mean. For both additive and multiplicative mixing, we use coefficients that are not convex combinations but rather conic combinations. Thus, additive and multiplicative mixing are performed with exponents and weights sampled from a Beta distribution independently.

```python
def pixmix(x_orig, x_mixing_pic, k=4, beta=3):
    x_pixmix = random.choice([augment(x_orig), x_orig])

    # random count of mixing rounds
    for i in range(random.choice([0,1,...,k])):

        # mixing_pic is from the mixing set
        # (e.g., fractal, natural image, etc.)
        mix_image = random.choice([augment(x_orig), x_mixing_pic])
        mix_op = random.choice([additive, multiplicative])

        x_pixmix = mix_op(x_pixmix, mix_image, beta)

    return x_pixmix

def augment(x):
    aug_op = random.choice([rotate, solarize, ..., posterize])
    return aug_op(x)
```

Figure 2: Simplified code for PIXMIX, our proposed data augmentation method. Initial images are mixed with a randomly selected image from our mixing set or augmentations of the clean image. The mixing operations are selected at random, and the mixing set includes fractals and feature visualization pictures.

3 Experiments

3.1 Tasks and Metrics

We compare PIXMIX to methods on five distinct ML Safety tasks. Individual methods are trained on clean versions of CIFAR-10, CIFAR-100, and ImageNet. Then, they are evaluated on each of the following tasks.

Corruptions. This task is to classify corrupted images from the CIFAR-10-C, CIFAR-100-C, and ImageNet-C datasets. The metric is the mean corruption error (mCE) across all fifteen corruptions and five severities for each corruption. Lower is better.

Consistency. This task is to consistently classify sequences of perturbed images from CIFAR-10-P, CIFAR-100-P, and ImageNet-P. The main metric is the mean flip rate (mFR), which corresponds to the probability that adjacent images in a temporal sequence have different predicted classes. This can be written as $\mathbb{P}_{x \sim \mathcal{S}}(f(x_j) \neq f(x_{j-1}))$, where x_i is the ith image in a sequence. For non-temporal sequences such as increasing noise values in a sequence $\mathcal{S}$, the metric is modified to $\mathbb{P}_{x \sim \mathcal{S}}(f(x_j) \neq f(x_1))$. Lower is better.

Adversaries. This task is to classify images that have been adversarially perturbed by projected gradient descent (Madry et al., 2018). For this task, we focus on untargeted perturbations on CIFAR-10 and CIFAR-100 with an ℓ_∞ budget of 2/255 and 20 steps of optimization. We do not display results of ImageNet models against adversaries in our tables, as for all tested methods the accuracy declines to zero with this budget. The metric is the classifier error rate. Lower is better.

Calibration. This task is to classify images with calibrated prediction probabilities, i.e. matching the empirical frequency of correctness. For example, if a weather forecast predicts that it will rain with 70% probability on ten occasions, then we would like the model to be correct 7/10 times. Formally, we want posteriors from a model f to satisfy $\mathbb{P}\left(Y = \arg\max_i f(X)_i \mid \max_i f(X)_i = C\right) = C$, where X, Y are random variables representing the data distribution. The metric is RMS calibration error (Hendrycks et al., 2019c), which is computed as $\sqrt{\mathbb{E}_C[(\mathbb{P}(Y = \hat{Y}|C = c) - c)^2]}$, where C is the classifier's confidence that its prediction $\hat{Y}$ is correct. We use adaptive binning (Nguyen and O'Connor, 2015b) to compute this metric. Lower is better.

Anomaly Detection. In this task we detect out-of-distribution (Hendrycks and Gimpel, 2017) or out-of-class images from various unseen distributions. The anomaly distributions are Gaussian,

Rademacher, Blobs, Textures (Cimpoi et al., 2014), SVHN (Netzer et al., 2011), LSUN (Yu et al., 2015), Places69 (Zhou et al., 2017). We describe each in the Appendix and report average AUROC. An AUROC of 50% is random chance and 100% is perfect detection. Higher is better.

3.2 Results on CIFAR-10/100 Tasks

Training Setup. In the following CIFAR experiments, we train a 40-4 Wide ResNet (Zagoruyko and Komodakis, 2016) with a drop rate of 0.3 for 100 epochs. All experiments use an initial learning rate of 0.1 which decays following a cosine learning rate schedule (Loshchilov and Hutter, 2016). For PIXMIX experiments, we use $k = 4, \beta = 3$. Hyperparameter robustness is discussed in the Appendix. Additionally, we use a weight decay of 0.0001 for Mixup and 0.0005 otherwise.

Results. In Table 1, we see that PIXMIX improves over the standard baseline method on all safety measures. Moreover, all other methods decrease performance relative to the baseline for at least one metric, while PIXMIX is the first method to improve performance in all settings. Results for all other methods are in Table 2. PIXMIX obtains better performance than all methods on Corruptions, Consistency, Adversaries, and Calibration. Notably, PIXMIX is far better than other methods for improving confidence calibration, reaching acceptably low calibration error on CIFAR-10. For corruption robustness, performance improvements on CIFAR-100 are especially large, with mCE on the Corruptions task dropping by 4.9% compared to AugMix and 19.5% compared to the baseline.

In addition to robustness and calibration, PIXMIX also greatly improves anomaly detection. PIXMIX nearly matches the anomaly detection performance of Outlier Exposure, the state-of-the-art anomaly detection method, without requiring large quantities of diverse, known outliers. This is surprising, as PIXMIX uses a standard cross-entropy loss, which makes the augmented images seem more in-distribution. Hence, one might expect unseen corruptions to be harder to distinguish as well, but in fact we observe the opposite—anomalies are easier to distinguish. Additional results and ablations are in the Appendix.

		Baseline	Cutout	Mixup	CutMix	Auto Augment	AugMix	Outlier Exposure	PIXMIX
CIFAR-10	Corruptions	26.4	25.9	21.0	26.5	22.2	12.4	25.1	**9.5**
	Consistency	3.4	3.7	2.9	3.5	3.6	1.7	3.4	**1.7**
	Adversaries	91.3	96.0	93.3	92.1	95.1	86.8	92.9	**82.1**
	Calibration	22.7	17.8	12.1	18.6	14.8	9.4	13.0	**3.7**
	Anomaly Detection (↑)	91.9	91.4	88.2	92.0	93.2	89.2	**98.4**	97.0
CIFAR-100	Corruptions	50.0	51.5	48.0	51.5	47.0	35.4	51.5	**30.5**
	Consistency	10.7	11.9	9.5	12.0	11.2	6.5	11.3	**5.7**
	Adversaries	96.8	98.5	97.4	97.0	98.1	95.6	97.2	**92.9**
	Calibration	31.2	31.1	13.0	29.3	24.9	18.8	15.2	**8.1**
	Anomaly Detection (↑)	77.7	74.3	71.7	74.4	80.4	84.9	**90.3**	89.3

Table 2: On CIFAR-10 and CIFAR-100, PIXMIX outperforms state-of-the-art techniques on five distinct safety metrics. Lower is better except for anomaly detection, and full results are in the Supplementary Material.

4 Conclusion

We proposed PIXMIX, a simple and effective data augmentation technique for improving ML safety measures. Unlike previous data augmentation techniques, PIXMIX introduces new complexity into the training procedure by leveraging fractals and feature visualizations. We evaluated PIXMIX on numerous distinct ML Safety tasks: corruption robustness, rendition robustness, prediction consistency, adversarial robustness, confidence calibration, and anomaly detection. We found that PIXMIX was the first method to provide substantial improvements over the baseline on all existing safety metrics, and it obtained state-of-the-art performance in nearly all settings.

References

D. Anguelov. Machine learning for autonomous driving, 2019. URL https://www.youtube.com/watch?v=Q0nGo2-y0xY.

M. Baradad, J. Wulff, T. Wang, P. Isola, and A. Torralba. Learning to see by looking at noise. *arXiv preprint arXiv:2106.05963*, 2021.

D. Bashkirova, D. Hendrycks, D. Kim, S. Mishra, K. Saenko, K. Saito, P. Teterwak, and B. Usman. Visda-2021 competition universal domain adaptation to improve performance on out-of-distribution data. *arXiv preprint arXiv:2107.11011*, 2021.

S. Chun, S. J. Oh, S. Yun, D. Han, J. Choe, and Y. Yoo. An empirical evaluation on robustness and uncertainty of regularization methods. *Uncertainty and Robustness in Deep Learning. ICML Workshop*, 2019.

M. Cimpoi, S. Maji, I. Kokkinos, S. Mohamed, , and A. Vedaldi. Describing textures in the wild. In *Computer Vision and Pattern Recognition*, 2014.

E. D. Cubuk, B. Zoph, D. Mané, V. Vasudevan, and Q. V. Le. AutoAugment: Learning augmentation policies from data. *CVPR*, 2018.

J. Deng, W. Dong, R. Socher, L. jia Li, K. Li, and L. Fei-Fei. ImageNet: A large-scale hierarchical image database. *CVPR*, 2009.

T. Devries and G. W. Taylor. Improved regularization of convolutional neural networks with Cutout. *arXiv preprint arXiv:1708.04552*, 2017.

T. Devries and G. W. Taylor. Learning confidence for out-of-distribution detection in neural networks. *ArXiv*, abs/1802.04865, 2018.

A. Emmott, S. Das, T. Dietterich, A. Fern, and W.-K. Wong. A meta-analysis of the anomaly detection problem. *arXiv preprint arXiv:1503.01158*, 2015.

R. Geirhos, P. Rubisch, C. Michaelis, M. Bethge, F. A. Wichmann, and W. Brendel. Imagenet-trained CNNs are biased towards texture; increasing shape bias improves accuracy and robustness. *ICLR*, 2019.

C. Guo, G. Pleiss, Y. Sun, and K. Q. Weinberger. On calibration of modern neural networks. In *International Conference on Machine Learning*, pages 1321–1330. PMLR, 2017.

D. Hendrycks and T. Dietterich. Benchmarking neural network robustness to common corruptions and perturbations. *ICLR*, 2019.

D. Hendrycks and K. Gimpel. A baseline for detecting misclassified and out-of-distribution examples in neural networks. *ICLR*, 2017.

D. Hendrycks, K. Lee, and M. Mazeika. Using pre-training can improve model robustness and uncertainty. In *ICML*, 2019a.

D. Hendrycks, M. Mazeika, and T. Dietterich. Deep anomaly detection with outlier exposure. In *International Conference on Learning Representations*, 2019b. URL https://openreview.net/forum?id=HyxCxhRcY7.

D. Hendrycks, M. Mazeika, and T. Dietterich. Deep anomaly detection with outlier exposure. *ICLR*, 2019c.

D. Hendrycks, M. Mazeika, S. Kadavath, and D. Song. Using self-supervised learning can improve model robustness and uncertainty. *arXiv preprint arXiv:1906.12340*, 2019d.

D. Hendrycks, N. Mu, E. D. Cubuk, B. Zoph, J. Gilmer, and B. Lakshminarayanan. Augmix: A simple data processing method to improve robustness and uncertainty. *arXiv preprint arXiv:1912.02781*, 2019e.

D. Hendrycks, S. Basart, N. Mu, S. Kadavath, F. Wang, E. Dorundo, R. Desai, T. Zhu, S. Parajuli, M. Guo, D. Song, J. Steinhardt, and J. Gilmer. The many faces of robustness: A critical analysis of out-of-distribution generalization. *ICCV*, 2021a.

D. Hendrycks, N. Carlini, J. Schulman, and J. Steinhardt. Unsolved problems in ml safety. *arXiv preprint arXiv:2109.13916*, 2021b.

H. Kataoka, K. Okayasu, A. Matsumoto, E. Yamagata, R. Yamada, N. Inoue, A. Nakamura, and Y. Satoh. Pre-training without natural images. In *Proceedings of the Asian Conference on Computer Vision*, 2020.

P. W. Koh, S. Sagawa, H. Marklund, S. M. Xie, M. Zhang, A. Balsubramani, W. hua Hu, M. Yasunaga, R. L. Phillips, S. Beery, J. Leskovec, A. Kundaje, E. Pierson, S. Levine, C. Finn, and P. Liang. Wilds: A benchmark of in-the-wild distribution shifts. In *ICML*, 2021.

B. Lakshminarayanan, A. Pritzel, and C. Blundell. Simple and scalable predictive uncertainty estimation using deep ensembles. In *NeurIPS*, 2017.

K. Lee, H. Lee, K. Lee, and J. Shin. Training confidence-calibrated classifiers for detecting out-of-distribution samples. *ICLR*, 2018a.

K. Lee, K. Lee, H. Lee, and J. Shin. A simple unified framework for detecting out-of-distribution samples and adversarial attacks. *NeurIPS*, 2018b.

S. Liang, Y. Li, and R. Srikant. Enhancing the reliability of out-of-distribution image detection in neural networks. *ICLR*, 2018.

S. Lloyd. Measures of complexity: a nonexhaustive list. *IEEE Control Systems Magazine*, 21(4):7–8, 2001.

R. G. Lopes, D. Yin, B. Poole, J. Gilmer, and E. D. Cubuk. Improving robustness without sacrificing accuracy with patch Gaussian augmentation. *arXiv preprint arXiv:1906.02611*, 2019.

I. Loshchilov and F. Hutter. SGDR: stochastic gradient descent with warm restarts. *ICLR*, 2016.

A. Madry, A. Makelov, L. Schmidt, D. Tsipras, and A. Vladu. Towards deep learning models resistant to adversarial attacks. *arXiv preprint arXiv:1706.06083*, 2017.

A. Madry, A. Makelov, L. Schmidt, D. Tsipras, and A. Vladu. Towards deep learning models resistant to adversarial attacks. *ICLR*, 2018.

E. Mintun, A. Kirillov, and S. Xie. On interaction between augmentations and corruptions in natural corruption robustness. *arXiv preprint arXiv:2102.11273*, 2021.

A. Mordvintsev, C. Olah, and M. Tyka. Inceptionism: Going deeper into neural networks, 2015. URL https://research.googleblog.com/2015/06/inceptionism-going-deeper-into-neural.html.

K. Nakashima, H. Kataoka, A. Matsumoto, K. Iwata, and N. Inoue. Can vision transformers learn without natural images? *ArXiv*, abs/2103.13023, 2021.

Y. Netzer, T. Wang, A. Coates, A. Bissacco, B. Wu, and A. Y. Ng. Reading digits in natural images with unsupervised feature learning. In *NIPS Workshop on Deep Learning and Unsupervised Feature Learning*, 2011.

K. Nguyen and B. O'Connor. Posterior calibration and exploratory analysis for natural language processing models. *arXiv preprint arXiv:1508.05154*, 2015a.

K. Nguyen and B. T. O'Connor. Posterior calibration and exploratory analysis for natural language processing models. In *EMNLP*, 2015b.

C. Olah, A. Mordvintsev, and L. Schubert. Feature visualization. *Distill*, 2017. doi: 10.23915/distill.00007. https://distill.pub/2017/feature-visualization.

Y. Ovadia, E. Fertig, J. Ren, Z. Nado, D. Sculley, S. Nowozin, J. V. Dillon, B. Lakshminarayanan, and J. Snoek. Can you trust your model's uncertainty? Evaluating predictive uncertainty under dataset shift. *NeurIPS*, 2019.

L. Ruff, J. R. Kauffmann, R. A. Vandermeulen, G. Montavon, W. Samek, M. Kloft, T. G. Dietterich, and K.-R. Müller. A unifying review of deep and shallow anomaly detection. *Proceedings of the IEEE*, 2021.

E. Rusak, L. Schott, R. S. Zimmermann, J. Bitterwolf, O. Bringmann, M. Bethge, and W. Brendel. A simple way to make neural networks robust against diverse image corruptions. In *European Conference on Computer Vision*, pages 53–69. Springer, 2020.

S. Sagawa, P. W. Koh, T. B. Hashimoto, and P. Liang. Distributionally robust neural networks for group shifts: On the importance of regularization for worst-case generalization. *ICLR*, 2020.

A. Steiner, A. Kolesnikov, X. Zhai, R. Wightman, J. Uszkoreit, and L. Beyer. How to train your vit? data, augmentation, and regularization in vision transformers. *arXiv preprint arXiv:2106.10270*, 2021.

R. Takahashi, T. Matsubara, and K. Uehara. Data augmentation using random image cropping and patching for deep cnns. *IEEE Transactions on Circuits and Systems for Video Technology*, 30(9): 2917–2931, 2019.

Tesla. Tesla ai day, 2021. URL https://www.youtube.com/watch?v=j0z4FweCy4M.

Y. Tokozume, Y. Ushiku, and T. Harada. Between-class learning for image classification. In *Proceedings of the IEEE Conference on Computer Vision and Pattern Recognition*, pages 5486–5494, 2018.

D. Tsipras, S. Santurkar, L. Engstrom, A. Turner, and A. Madry. Robustness may be at odds with accuracy. *arXiv preprint arXiv:1805.12152*, 2018.

D. Yin, R. G. Lopes, J. Shlens, E. D. Cubuk, and J. Gilmer. A fourier perspective on model robustness in computer vision. *NeurIPS*, 2019.

F. Yu, Y. Zhang, S. Song, A. Seff, and J. Xiao. LSUN: construction of a large-scale image dataset using deep learning with humans in the loop. *CoRR*, 2015.

S. Yun, D. Han, S. J. Oh, S. Chun, J. Choe, and Y. Yoo. Cutmix: Regularization strategy to train strong classifiers with localizable features. *ICCV*, 2019.

S. Zagoruyko and N. Komodakis. Wide residual networks. In *BMVC*, 2016.

H. Zhang, M. Cissé, Y. Dauphin, and D. Lopez-Paz. mixup: Beyond empirical risk minimization. *ICLR*, 2017.

Z. Zhong, L. Zheng, G. Kang, S. Li, and Y. Yang. Random erasing data augmentation. *arXiv preprint arXiv:1708.04896*, 2017.

B. Zhou, A. Lapedriza, A. Khosla, A. Oliva, and A. Torralba. Places: A 10 million image database for scene recognition. *PAMI*, 2017.
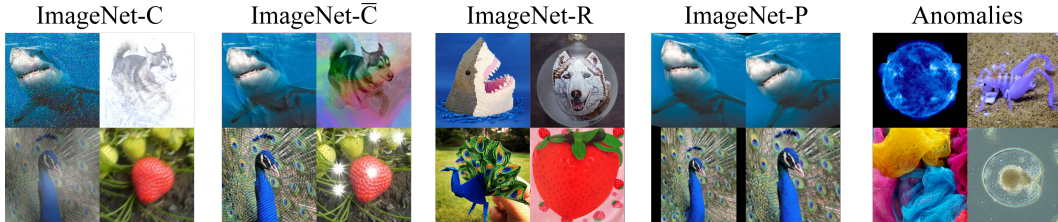
| ImageNet-C | ImageNet-$\overline{\text{C}}$ | ImageNet-R | ImageNet-P | Anomalies |

Figure 3: We comprehensively evaluate models across safety tasks, including corruption robustness (ImageNet-C, ImageNet-$\overline{\text{C}}$), rendition robustness (ImageNet-R), prediction consistency (ImageNet-P), confidence calibration, and anomaly detection. ImageNet-C (Hendrycks and Dietterich, 2019) contains 15 common corruptions, including fog, snow, and motion blur. ImageNet-$\overline{\text{C}}$ (Mintun et al., 2021) contains additional corruptions. ImageNet-R (Hendrycks et al., 2021a) contains renditions of object categories and measures robustness to shape abstractions. ImageNet-P (Hendrycks and Dietterich, 2019) contains sequences of gradual perturbations to images, across which predictions should be consistent. Anomalies are semantically distinct from the training classes. Existing work focuses on learning representations that improve performance on one or two metrics, often to the detriment of others. Developing models that perform well across multiple safety metrics is an important next step.

A Related Work

Datasets. We evaluate PIXMIX on extensions of CIFAR-10, CIFAR-100, and ImageNet-1K (henceforth referred to as ImageNet) for various safety tasks. So as not to ignore performance on the original tasks, we also evaluate on the standard versions of these datasets. ImageNet consists of 1.28 million color images. As is common practice, we downsample ImageNet images to 224×224 resolution in all experiments. ImageNet consists of 1,000 classes from WordNet noun synsets, covering a wide variety of objects, including fine-grained distinctions. We use the validation set for evaluating clean accuracy, which contains 50,000 images.

To measure corruption robustness, we use the CIFAR-10-C, CIFAR-100-C, and ImageNet-C datasets (Hendrycks and Dietterich, 2019). Each dataset consists of 15 diverse corruptions applied to each image in the original test set. The corruptions can be grouped into blur, weather, and digital corruptions. Each corruption appears at five levels of severity. We also evaluate on the similar CIFAR-10-$\overline{\text{C}}$ and ImageNet-$\overline{\text{C}}$ datasets, which use a different set of corruptions (Mintun et al., 2021). To measure robustness to different renditions of object categories, we use the ImageNet-R dataset (Hendrycks et al., 2021a). These datasets enable evaluating the out-of-distribution generalization of classifiers trained on clean data and non-overlapping augmentations.

To measure consistency of predictions, we use the CIFAR-10-P, CIFAR-100-P, and ImageNet-P datasets. Each dataset consists of 10 gradual shifts that images can undergo, such as zoom, translation, and brightness variation. Unlike other datasets we evaluate on, each example in these datasets is a video, and the objective is to have robust predictions that do not change across per-frame perturbations. These datasets enable measuring the stability, volatility, or "jaggedness" of network predictions in the face of minor perturbations. Examples from these datasets are in Figure 3.

Methods. We compare PIXMIX to various state-of-the-art data augmentation methods. *Baseline* denotes standard data augmentation; for ImageNet, we use the a random resized crop and random horizontal flipping, while on CIFAR-10 and CIFAR-100, we use random cropping with zero padding followed by random horizontal flips. *Cutout* aims to improve representations by randomly masking out image patches, using patch side lengths that are half the side length of the original image. *Mixup* regularizes networks to behave linearly between training examples by training on pixel-wise linear interpolations between input images and labels. *CutMix* combines the techniques of Cutout and Mixup by replacing image patches with patches from other images in the training set. The labels of the resulting images are combined in proportion to the pixels taken by each source image. *Auto Augment* searches for compositions of augmentations that maximize accuracy on a validation set. *AugMix* uses a ResNeXt-like pipeline to combine randomly augmented images. Compared to AugMix, which requires up to 9 augmentations per image and can be slow to run, PIXMIX requires substantially fewer augmentations; we find an average of 2 augmentations is sufficient. For fairness, we follow

(Mintun et al., 2021) and train AugMix without the Jensen-Shannon Divergence consistency loss, which requires at least thrice the memory per batch. *Outlier Exposure* trains networks to be uncertain on a training dataset of outliers, and these outliers are distinct from the out-of-distribution test sets that we use during evaluation. For ImageNet experiments, we compare to several additional methods. *SIN* trains networks on a mixture of clean images and images rendered using neural style transfer (Geirhos et al., 2019). We opt for simple techniques that are widely used and do not evaluate all possible techniques from each of the areas we consider. More methods are evaluated in the Appendix.

Robustness. Out-of-distribution robustness considers how to make ML models resistant to various forms of data shift at test time. Geirhos et al., 2019 (Geirhos et al., 2019) uncover a texture bias in convolutional networks and show that training on diverse stylized images can improve robustness at test-time. The ImageNet-C(orruptions) benchmark (Hendrycks and Dietterich, 2019) consists of diverse image corruptions known to track robustness on some real world data shifts (Hendrycks et al., 2021a). ImageNet-C is used to test models that are trained on ImageNet (Deng et al., 2009) and is used as a held-out, more difficult test set. They also introduce ImageNet-P(erturbations) for measuring prediction consistency under various non-adversarial input perturbations. Others have introduced additional corruptions for evaluation called ImageNet-$\overline{\text{C}}$ (Mintun et al., 2021). The ImageNet-R(enditions) benchmark measures performance degradation under various renditions of objects including paintings, cartoons, graffiti, embroidery, origami, sculptures, toys, and more (Hendrycks et al., 2021a). In the similar setting of domain adaptation, Bashkirova et al., 2021 (Bashkirova et al., 2021) consider evaluating test-time robustness of models and even anomaly detection (Emmott et al., 2015; Liang et al., 2018; Ruff et al., 2021). Yin et al., 2019 (Yin et al., 2019) show that adversarial training can substantially reduce robustness on some corruptions and argue that part of model fragility is explained by overreliance on spurious cues (Sagawa et al., 2020; Koh et al., 2021).

Calibration. Calibrated prediction confidences are valuable for classification models in real-world settings. Several works have investigated evaluating and improving the calibration of deep neural networks (Nguyen and O'Connor, 2015a; Guo et al., 2017) through the use of validation sets. Others have shown that calibration can be improved without a validation set through methods such as ensembling (Lakshminarayanan et al., 2017) and pre-training (Hendrycks et al., 2019a). Ovadia et al. (Ovadia et al., 2019) find that models are markedly less calibrated under distribution shift.

Anomaly Detection. Since models should ideally know what they do not know, they will need to identify when an example is anomalous. Anomaly detection seeks to estimate whether an input is out-of-distribution (OOD) with respect to a given training set. Hendrycks et al., 2017 (Hendrycks and Gimpel, 2017) propose a simple baseline for detecting classifier errors and OOD inputs. Devries et al., 2018 (Devries and Taylor, 2018) propose training classifiers with an additional confidence branch for detecting OOD inputs. Lee et al., 2018 (Lee et al., 2018a) propose improving representations used for detectors with near-distribution images generated by GANs. Lee et al., 2018 (Lee et al., 2018b) also propose the Mahalanobis detector. Outlier Exposure (Hendrycks et al., 2019b) fine-tunes classifiers with diverse, natural anomalies, and since it is the state-of-the-art for OOD detection, we test this method in our paper.

Data Augmentation. Simulated and augmented inputs can help make ML systems more robust, and this approach is used in real-world applications such as autonomous driving (Tesla, 2021; Anguelov, 2019). For state-of-the-art models, data augmentation can improve clean accuracy comparably to a $10\times$ increase in model size (Steiner et al., 2021). Further, data augmentation can improve out-of-distribution robustness comparably to a $1{,}000\times$ increase in labeled data (Hendrycks et al., 2021a). Various augmentation techniques for image data have been proposed, including Cutout (Devries and Taylor, 2017; Zhong et al., 2017), Mixup (Zhang et al., 2017; Tokozume et al., 2018), CutMix (Yun et al., 2019; Takahashi et al., 2019), and AutoAugment (Cubuk et al., 2018; Yin et al., 2019). Lopes et al., 2019 (Lopes et al., 2019) find that inserting random noise patches into training images improves robustness. AugMix is a data augmentation technique that specifically improves OOD generalization (Hendrycks et al., 2019e). Chun et al. (Chun et al., 2019) evaluates some of these techniques on CIFAR-10-C, a variant of ImageNet-C for the CIFAR-10 dataset (Hendrycks and Dietterich, 2019). They find that these data augmentation techniques can improve OOD generalization at the cost of weaker OOD detection.

Analyzing Safety Goals Simultaneously. Recent works study how a given method influences safety goals (Hendrycks et al., 2021b) simultaneously. Prior work has shown that Mixup, CutMix, Cutout, ShakeDrop, adversarial training, Gaussian noise augmentation, and more have mixed effects

on various safety metrics (Chun et al., 2019). Others have shown that different pretraining methods can improve some safety metrics and hardly affect others, but the pretraining method must be modified per task (Hendrycks et al., 2019a). Self-supervised learning methods can also be repurposed to help with some safety goals, all while not affecting others, but to realize the benefit, each task requires different self-supervised learning models (Hendrycks et al., 2019d). Thus, creating a single method for improving performance across multiple safety metrics is an important next step.

Training on Complex Synthetic Images.   Kataoka et al., 2020 (Kataoka et al., 2020) introduce FractalDB, a dataset of black-and-white fractals, and they show that pretraining on these algorithmically generated fractal images can yield better downstream performance than pretraining on many manually annotated natural datasets. Nakashima et al. (Nakashima et al., 2021) show that models trained on a large variant of FractalDB can match ImageNet-1K pretraining on downstream tasks. Baradad et al., 2021 (Baradad et al., 2021) find that, for self-supervised learning, other synthetic datasets may be more effective than FractalDB, and they find that structural complexity and diversity are key properties for good downstream transfer. We depart from this recent line of work and ask whether structurally complex images can be repurposed for data augmentation instead of training from scratch. While data augmentation techniques such as those that add Gaussian noise increase input entropy, such noise has maximal *descriptive* complexity but introduce little *structural* complexity (Lloyd, 2001). Since a popular definition of structural complexity is the fractal dimension (Lloyd, 2001), we turn to fractals and other structurally complex images for data augmentation.

B Additional Results

	Accuracy	Robustness			Consistency		Calibration				Anomaly Detection	
	Clean	C	$\overline{\text{C}}$	R	ImageNet-P		Clean	C	$\overline{\text{C}}$	R	Out-of-Class Datasets	
	Error	mCE	Error	Error	mFR	mT5D	RMS	RMS	RMS	RMS	AUROC (↑)	AUPR (↑)
Baseline	23.9	78.2	61.0	63.8	58.0	78.4	5.6	12.0	20.7	19.7	79.7	48.6
Cutout	<u>22.6</u>	76.9	60.2	64.8	57.9	75.2	3.8	11.1	17.1	14.6	81.7	49.6
Mixup	22.7	72.7	55.0	62.3	54.3	73.2	5.8	7.3	13.2	44.6	72.2	51.3
CutMix	22.9	77.8	59.8	66.5	60.3	76.6	6.2	9.1	15.3	43.5	78.4	47.9
AutoAugment	**22.4**	73.8	58.0	61.9	54.2	72.0	**3.6**	8.0	14.3	12.6	84.4	58.2
AugMix	22.8	71.0	56.5	61.7	52.7	70.9	4.5	9.2	15.0	13.2	84.2	61.1
SIN	25.4	70.9	57.6	**58.5**	54.4	71.8	4.2	6.5	14.0	16.2	84.8	62.3
PIXMIX	<u>22.6</u>	**65.8**	**44.3**	<u>60.1</u>	**51.1**	**69.1**	**3.6**	**6.3**	**5.8**	**11.0**	**85.7**	**64.1**

Table 3: On ImageNet, PIXMIX improves over state-of-the-art methods on a broad range of safety metrics. Lower is better except for anomaly detection, and the full results are in the Supplementary Material. **Bold** is best, and <u>underline</u> is second best. Across evaluation settings, PIXMIX is occasionally second-best, but it is usually first, making it near Pareto-optimal.

B.1 Results on ImageNet Tasks

Training Setup. Since regularization methods may require a greater number of training epochs to converge, we fine-tune a pre-trained ResNet-50 for 90 epochs. For PIXMIX experiments, we use $k = 4, \beta = 4$. We use a batch size of 512 and an initial learning rate of 0.01 following a cosine decay schedule.

Results. We show ImageNet results in Table 3. Compared to the standard augmentations of the baseline, PIXMIX has higher performance on all safety measures. By contrast, other augmentation methods have lower performance than the baseline (cropping and flipping) on some metrics. Thus, PIXMIX is the first augmentation method with a Pareto improvement over the baseline on a broad range of safety measures.

On corruption robustness, PIXMIX outperforms state-of-the-art augmentation methods such as AugMix, improving mCE by 12.4% over the baseline and 5.1% over the mCE of the next-best method. On rendition robustness, PIXMIX outperforms all other methods save for SIN. Note that SIN is particularly well-suited to improving rendition robustness, as it trains on stylized ImageNet data. However, SIN incurs a 2% loss to clean accuracy, while PIXMIX increases clean accuracy by 1.3%. Maintaining strong performance on clean images is an important property for methods to have, as practitioners may be unwilling to adopt methods that markedly reduce performance in ideal conditions.

On calibration tasks, PIXMIX outperforms all methods. As Ovadia et al. (Ovadia et al., 2019) show, models are markedly less calibrated under distribution shift. We find that PIXMIX cuts calibration error in half on ImageNet-C compared to the baseline. On ImageNet-C, the improvement is even larger, with a 14.9% reduction in absolute error. In Figure 4, we visualize how calibration error on ImageNet-C and ImageNet-C varies as the corruption severities increase. Compared to the baseline, PIXMIX calibration error increases much more slowly. Further uncertainty estimation results are in the Appendix. For example, PIXMIX substantially improves anomaly detection performance with Places365 as the in-distribution set.

B.2 Mixing Set Picture Source Ablations

While we provide a high-quality source of structural complexity with PIXMIX, our mixing pipeline could be used with other mixing sets. In Table 4, we analyze the choice of mixing set on CIFAR-100 performance. We replace our Fractals and Feature Visualizations dataset (Fractals + FVis) with several synthetic datasets developed for unsupervised representation learning (Baradad et al., 2021; Kataoka et al., 2020). We also evaluate the 300K Random Images dataset of natural images used for Outlier Exposure on CIFAR-10 and CIFAR-100 (Hendrycks et al., 2019c).

Compared to alternative sources of visual structure, the Fractals + FVis mixing set yields substantially better results. This suggests that structural complexity in the mixing set is important. Indeed, the
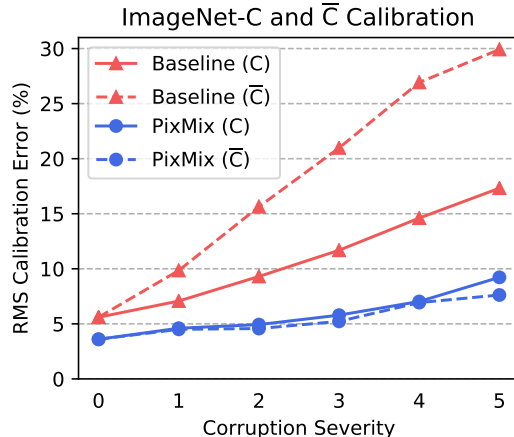
Figure 4: As corruption severity increases, PIXMIX calibration error increases much more slowly than the baseline calibration error, demonstrating that PIXMIX can improve uncertainty estimation under distribution shifts with unseen image corruptions.

| | Accuracy | Corruptions | Consistency | Adversaries | Calibration | Anomaly |
| | Clean | C | CIFAR-P | PGD | C | Detection |
PIXMIX Mixing Set	Error	mCE	mFR	Error	RMS	AUROC (↑)
Dead Leaves (Squares)	21.3	36.2	6.3	94.1	15.8	81.8
Spectrum + Color + WMM	20.7	36.1	6.6	94.4	15.9	85.8
StyleGAN (Oriented)	20.4	37.3	7.2	97.0	14.9	83.7
FractalDB	<u>20.3</u>	33.9	6.4	98.2	12.0	82.5
300K Random Images	**19.6**	34.5	6.3	94.7	12.9	86.2
Fractals	<u>20.3</u>	32.3	6.2	95.5	<u>8.7</u>	<u>88.9</u>
Feature Visualization (FVis)	21.5	**30.3**	**5.4**	**91.5**	9.9	88.1
Fractals + FVis	<u>20.3</u>	<u>30.5</u>	<u>5.7</u>	<u>92.9</u>	**8.1**	**89.3**

Table 4: Mixing set ablations showing that PIXMIX can use numerous mixing sets, including real images. Results are using CIFAR-100. **Bold** is best, and <u>underline</u> is second best. We compare Fractals + FVis, the mixing set used as PIXMIX's default mixing set, to other datasets from prior works (Baradad et al., 2021; Kataoka et al., 2020). The 300K Random Images (Hendrycks et al., 2019c) are real images scraped from online for Outlier Exposure. We discover the distinct utility of Fractals and FVis. By utilizing the 300K Random Images mixing set, PIXMIX can attain a 19.6% error rate, though fractals can provide more robustness than these real images.

next-best method for reducing mCE on CIFAR-100-C is FractalDB, which consists of weakly curated black-and-white fractal images. By contrast, our Fractals dataset consists of color images of fractals that were manually designed and curated for being visually interesting. Furthermore, we find that removing either Fractals or FVis from the mixing set yields lower performance on safety metrics or lower performance on clean data, showing that both components of our mixing set are important.

Mixing Strategies. In Table 5, we analyze different mixing strategies. The full PIXMIX mixing strategy is depicted in Figures 2 and 3 of the main paper. Mix Input only includes clean images in the mixing pipeline and does not use the mixing set at all. This severely harms performance on all safety metrics. Mix Aug only mixes with images from the mixing set. This reduces RMS calibration error but increases error on robustness tasks compared to PIXMIX Original. Finally, Iterative mixes with feature visualizations computed on the fly for the network being trained. This performs well on robustness tasks but has weaker calibration and anomaly detection. Additionally, computing feature visualizations at each iteration of training is substantially slower than precomputing them on fixed networks as we do in PIXMIX.

Full Results. In Tables 7, 8, and 9, we report full results for CIFAR-10, CIFAR-100, and ImageNet. The ImageNet results are copied from the main paper. For CIFAR, we evaluate on additional datasets, including CIFAR-10-C and CIFAR-100-C, additional datasets of corrupted CIFAR images. We also report the mT5D metric on ImageNet-P. In all cases, PIXMIX provides the best overall performance.

13

Noise-Based Augmentations. Since noise-based augmentations sometimes nearly overlap with the test distribution and thereby may have an unfair advantage, we separately compare to several additional baselines on ImageNet that use noise-based data augmentations. *ANT* trains networks on inputs with adversarially transformed noise applied (Rusak et al., 2020). *Speckle* trains on inputs with speckle noise added, which has been observed to improve robustness. *EDSR* and *Noise2Net* inject noise using image-to-image neural networks with noisy parameters (Hendrycks et al., 2021a). *Adversarial* trains networks with ℓ_∞ perturbations of magnitude $\varepsilon = 8/255$ (Madry et al., 2017).

Results are in Tables 10. We find that ANT and Speckle have strong performance on ImageNet-P overall, but this mostly comes from the Gaussian and shot noise categories. If we only consider prediction stability on non-noise categories, PIXMIX exhibits the least volatility in predictions out of all the methods considered.

Hyperparameter Sensitivity. In Table 13, we examine the hyperparameter sensitivity of PIXMIX on corruption robustness for CIFAR-100. We vary the β and k hyperparameters and find that performance is very stable across a range of hyperparameters.

Places365 Anomaly Detection. In Table 12, we show anomaly detection performance with Places365 as the in-distribution data. For all methods, we use a ResNet-18 pre-trained on Places365. PIXMIX and Outlier Exposure (OE) are fine-tuned for 10 epochs. We find that PIXMIX nearly matches the state-of-the-art OE detector despite being a general data augmentation technique that improves many other safety metrics.

C   Outlier Datasets

For anomaly detection, we use a suite of out-of-distribution datasets and average metrics across all OOD datasets in the main results. Gaussian noise is IID noise sampled from a normal distribution. Rademacher Noise is noise with each pixel sampled from $\{-1, 1\}$ with equal probability. Blobs are algorithmically generated blobs. Textures are from the Describable Textures Dataset (Cimpoi et al., 2014). SVHN has images of numbers from houses. Places69 contains 69 held-out classes.

D   Broader Impacts

As PIXMIX differentially improves safety metrics, it could have various beneficial effects. Improved robustness can result in more reliable machine learning systems deployed in safety-critical situations (Hendrycks et al., 2021b), such as self-driving cars. Anomaly detection enables better human oversight of machine learning systems and fallback policies in cases where systems encounter inputs they were not designed to handle. At the same time, anomaly detection could be misused as a surveillance tool, requiring careful consideration of individual use cases. Calibration enables more meaningful predictions that increase trust with end users. Additionally, compared to other methods for improving robustness, PIXMIX requires minimal modification of the training setup and a low computational overhead, resulting in lower costs to machine learning practitioners and the environment.

	Accuracy	Corruptions	Consistency	Adversaries	Calibration	Anomaly
	Clean	C	CIFAR-P	PGD	C	Detection
	Error ($\downarrow$)	mCE ($\downarrow$)	mFR ($\downarrow$)	Error ($\downarrow$)	RMS ($\downarrow$)	AUROC ($\uparrow$)
PIXMIX Original	20.3	30.5	5.7	92.9	8.1	89.3
Mix Input	19.9	34.1	6.4	96.7	15.5	86.5
Mix Aug	20.6	31.1	6.2	94.2	6.0	89.7
Iterative	21.1	31.4	5.6	90.6	12.7	86.7

Table 5: PIXMIX variations on CIFAR-100. Mix Input only mixes with augmented versions of the clean image. Mix Aug only mixes with images from the mixing set (i.e. fractals and feature visualizations). Iterative mixes with feature visualizations computed on the fly for the current network. Using the mixing set alone is more effective than augmented images alone, and combining them can further improve performance on several metrics.

	Accuracy	Corruptions		Consistency		Adversaries	Calibration			Anomaly	
	Clean	C	C̄	CIFAR-P		PGD	Clean	C	C̄	Detection	
	Error	mCE	mCE	mFR	mT5D	Error	RMS	RMS	RMS	AUROC (↑)	AUPR (↑)
CutMix	20.3	51.5	49.6	12.0	3.0	97.0	12.2	29.3	26.5	74.4	32.3
PIXMIX	20.3	**30.5**	36.7	**5.7**	**1.6**	**92.9**	7.0	8.1	8.9	89.3	**70.9**
PIXMIX + CutMix	**19.9**	30.9	**35.5**	5.8	1.7	93.1	**4.4**	**6.0**	**5.9**	**89.5**	68.6

Table 6: Combining PIXMIX and CutMix on CIFAR-100. While PIXMIX is strong on its own, combination with other data augmentation techniques can further improve performance.

	Accuracy	Corruptions		Consistency		Adversaries	Calibration			Anomaly	
	Clean	C	C̄	CIFAR-P		PGD	Clean	C	C̄	Detection	
	Error	mCE	mCE	mFR	mT5D	Error	RMS	RMS	RMS	AUROC (↑)	AUPR (↑)
Baseline	21.3	50.0	52.0	10.7	2.7	96.8	14.6	31.2	30.9	77.7	35.4
Cutout	19.9	51.5	50.2	11.9	2.7	98.5	11.4	31.1	29.4	74.3	31.3
Mixup	21.1	48.0	49.8	9.5	3.0	97.4	10.5	13.0	12.9	71.7	31.9
CutMix	20.3	51.5	49.6	12.0	3.0	97.0	12.2	29.3	26.5	74.4	32.3
AutoAugment	**19.6**	47.0	46.8	11.2	2.6	98.1	9.9	24.9	22.8	80.4	33.2
AugMix	20.6	35.4	41.2	6.5	1.9	95.6	12.5	18.8	22.5	84.9	53.8
OE	21.9	50.3	52.1	11.3	3.0	97.0	12.0	13.8	13.9	**90.3**	66.2
PIXMIX	20.3	**30.5**	**36.7**	**5.7**	**1.6**	**92.9**	**7.0**	**8.1**	**8.9**	89.3	**70.9**

Table 7: Full results for CIFAR-100. mT5D is an additional metric used for gauging prediction consistency in ImageNet-P, which we adapt to CIFAR-100. Note PIXMIX can achieve 19.6% error rate if it uses 300K Random Images as the Mixing Set, so PIXMIX can achieve the same accuracy as AutoAugment yet also do better on safety metrics.

	Accuracy	Corruptions		Consistency		Adversaries	Calibration			Anomaly	
	Clean	CIFAR-C	C̄	CIFAR-P		PGD	Clean	CIFAR-C	C̄	Detection	
	Error	mCE	mCE	mFR	mT5D	Error	RMS	RMS	RMS	AUROC (↑)	AUPR (↑)
Baseline	4.4	26.4	26.4	3.4	1.7	91.3	6.4	22.7	22.4	91.9	70.9
Cutout	**3.6**	25.9	24.5	3.7	1.7	96.0	3.3	17.8	17.5	91.4	63.6
Mixup	4.2	21.0	22.1	2.9	2.1	93.3	12.5	12.1	10.9	88.2	67.1
CutMix	4.0	26.5	25.4	3.5	2.1	92.1	5.0	18.6	17.8	92.0	65.5
AutoAugment	3.9	22.2	24.4	3.6	1.7	95.1	4.0	14.8	16.6	93.2	64.6
AugMix	4.3	12.4	16.4	1.7	1.2	86.8	5.1	9.4	12.6	89.2	61.5
OE	4.6	25.1	26.1	3.4	1.9	92.9	6.9	13.0	13.2	**98.4**	**92.5**
PIXMIX	4.2	**9.5**	**13.6**	**1.7**	**1.0**	**82.1**	**2.6**	**3.7**	**5.3**	97.0	88.4

Table 8: Full results for CIFAR-10. mT5D is an additional metric used for gauging prediction consistency in ImageNet-P, which we adapt to CIFAR-10.

	Accuracy	Robustness			Consistency		Calibration				Anomaly	
	Clean	C	C̄	R	ImageNet-P		Clean	C	C̄	R	Detection	
	Error	mCE	Error	Error	mFR	mT5D	RMS	RMS	RMS	RMS	AUROC (↑)	AUPR (↑)
Baseline	23.9	78.2	61.0	63.8	58.0	78.4	5.6	12.0	20.7	19.7	79.7	48.6
Cutout	<u>22.6</u>	76.9	60.2	64.8	57.9	75.2	3.8	11.1	17.1	14.6	81.7	49.6
Mixup	22.7	72.7	55.0	62.3	54.3	73.2	5.8	7.3	13.2	44.6	72.2	51.3
CutMix	22.9	77.8	59.8	66.5	60.3	76.6	6.2	9.1	15.3	43.5	78.4	47.9
AutoAugment	**22.4**	73.8	58.0	61.9	54.2	72.0	**3.6**	8.0	14.3	12.6	84.4	58.2
AugMix	22.8	71.0	56.5	61.7	52.7	70.9	4.5	9.2	15.0	13.2	84.2	61.1
SIN	25.4	70.9	57.6	**58.5**	54.4	71.8	4.2	6.5	14.0	16.2	84.8	62.3
PIXMIX	<u>22.6</u>	**65.8**	**44.3**	<u>60.1</u>	**51.1**	**69.1**	**3.6**	**6.3**	**5.8**	**11.0**	**85.7**	**64.1**

Table 9: Full results for ImageNet. mT5D is an additional metric used for gauging prediction consistency in ImageNet-P. **Bold** is best, and <u>underline</u> is second best.

	Accuracy	Robustness			Consistency		Calibration				Anomaly	
	Clean	C	$\overline{\text{C}}$	R	ImageNet-P		Clean	C	$\overline{\text{C}}$	R	Detection	
	Error	mCE	Error	Error	mFR	mT5D	RMS	RMS	RMS	RMS	AUROC (↑)	AUPR (↑)
Baseline	23.9	78.2	61.0	63.8	58.0	78.4	5.6	12.0	20.7	19.7	79.7	48.6
ANT	23.9	67.0	61.0	61.0	48.0	68.4	7.0	10.3	19.3	22.9	80.9	54.3
Speckle	24.2	72.7	62.1	62.1	51.2	70.6	5.6	11.6	19.8	20.9	79.7	53.3
Noise2Net	22.7	71.6	57.7	57.6	51.5	72.3	4.4	8.9	16.3	15.2	84.8	60.4
EDSR	23.5	65.4	54.7	60.3	44.6	63.3	4.5	8.4	15.7	16.7	71.7	36.3
ℓ_∞ Adversarial	45.5	92.6	68.0	65.2	38.5	41.5	15.5	10.2	15.1	10.2	69.8	26.4
ℓ_2 Adversarial	37.2	85.5	64.9	63.0	29.2	34.8	11.3	9.7	16.6	10.7	78.9	40.2

Table 10: While many noise-based augmentation methods often do well on ImageNet-C by targeting the noise corruptions, they do not reliably improve performance across many safety metrics.

			Noise		Blur		Weather		Digital			
	Clean	mFR	Gaussian	Shot	Motion	Zoom	Snow	Bright	Translate	Rotate	Tilt	Scale
Baseline	23.9	58.0	59	58	65	72	63	62	44	52	57	48
ANT	23.9	48.0	41	36	50	61	48	58	40	48	52	46
Speckle	24.2	51.2	38	28	60	67	58	65	43	51	54	48
Noise2Net	22.7	51.5	54	53	50	70	56	50	38	47	52	43
EDSR	23.5	44.6	37	35	48	56	46	56	38	44	44	43
ℓ_∞ Adversarial	45.5	38.5	43	56	24	33	15	80	20	34	33	46
ℓ_2 Adversarial	37.2	29.2	24	30	24	31	14	64	13	27	26	39

Table 11: ImageNet-P results. The mean flipping rate is the average of the flipping rates across all 10 perturbation types. Noise-based augmentation methods are less performant on non-noise distribution shifts.

	AUROC (↑)			AUPR (↑)		
	Baseline	OE	PIXMIX	Baseline	OE	PIXMIX
Gaussian Noise	72.2	93.5	100.0	23.5	54.1	100.0
Rademacher Noise	47.7	90.2	100.0	14.6	44.9	100.0
Blobs	41.9	100.0	100.0	13.0	99.4	100.0
Textures	66.6	91.4	80.3	24.6	75.7	56.2
SVHN	96.6	100.0	99.5	90.5	99.9	98.6
ImageNet	63.0	86.5	71.5	25.1	69.7	47.4
Places69	61.5	63.1	62.3	23.4	24.9	31.3
Average	64.2	89.2	87.6	30.7	66.9	76.2

Table 12: Out-of-Distribution detection results for a ResNet-18 pre-trained on Places365. PIXMIX and OE are finetuned for 10 epochs. Despite being a general data augmentation technique, PIXMIX is near the state-of-the-art in OOD detection.

	$k = 2$	$k = 3$	$k = 4$
$\beta = 5$	20.2	20.0	20.1
	31.6	31.1	30.8
$\beta = 4$	19.7	20.3	20.1
	31.3	30.9	30.7
$\beta = 3$	20.3	20.2	20.3
	31.2	30.7	30.5

Table 13: Performance is not strongly affected by hyperparameters. We include the CIFAR-100 test set error and the CIFAR-100-C mCE for each hyperparameter setting.

	Clean	mCE	Noise			Blur				Weather				Digital			
			Gauss.	Shot	Impulse	Defocus	Glass	Motion	Zoom	Snow	Frost	Fog	Bright	Contrast	Elastic	Pixel	JPEG
Baseline	23.9	78.2	78	80	80	79	90	81	80	80	78	69	62	75	88	76	78
Cutout	22.6	76.9	76	77	79	76	90	79	79	79	78	69	60	74	87	75	75
Mixup	22.7	72.7	69	72	73	76	90	77	78	73	68	62	59	64	86	71	73
CutMix	22.9	77.8	78	80	80	79	90	81	80	80	78	69	62	75	88	76	78
AutoAugment	22.4	73.8	71	72	75	75	90	78	79	73	74	64	55	68	87	73	71
AugMix	22.8	71.0	69	70	70	72	88	74	71	73	74	58	58	59	85	73	72
SIN	25.4	70.9	64	65	66	73	84	73	80	71	74	66	62	69	80	64	73
PixMix	22.6	**65.8**	53	52	51	73	88	77	77	62	64	58	56	53	85	69	70

Table 14: Clean Error, mCE, and Corruption Error (CE) values for various methods on ImageNet-C. The mCE value is computed by averaging across per corruption CE values.

	Clean	$\overline{\text{C}}$ Error	BSmpl	Plsm	Ckbd	CSin	SFreq	Brown	Perlin	Sparkles	ISparkle	Refraction
Baseline	23.9	61.0	62	77	55	86	80	45	41	38	78	48
Cutout	22.6	60.2	64	77	49	85	80	45	41	36	77	47
Mixup	22.7	55.0	58	68	49	80	72	38	36	35	71	**44**
CutMix	22.9	59.8	64	77	**47**	85	80	46	41	35	75	47
AutoAugment	22.4	58.0	56	71	49	86	77	42	39	36	77	47
AugMix	22.8	56.5	51	71	48	83	76	42	38	36	75	45
SIN	25.4	57.6	53	72	54	81	68	41	41	41	79	47
PixMix	22.6	**44.3**	**40**	**48**	48	**48**	**47**	**34**	**37**	**33**	**65**	**44**

Table 15: Results for various methods on ImageNet-$\overline{\text{C}}$.